Anat Sci Int (2014) 89:171–182
DOI 10.1007/s12565-013-0216-8

ORIGINAL ARTICLE

A morphological study of the multi infraorbital canals of the maxilla in the Japanese macaque by cone-beam computed tomography

Tomonori Zaizen · Iwao Sato

Received: 17 July 2013 / Accepted: 1 November 2013 / Published online: 24 November 2013

Abstract The infraorbital canal in the Japanese macaque is composed of main and accessory canals. However, the morphological features of the infraorbital canal, such as the canal course and the supply of infraorbital vessels and nerves in the maxilla, are poorly characterized. In this study, we show the structure of the infraorbital canal of the Japanese macaque (adults; 10 male, 9 female), including the distribution of these vessels and nerves, using cone-beam computed tomography and a macroscopic apparatus. The superior and lateral margins of the orbit were correlated with the infraorbital canal on three-dimensional reconstruction images ($P < 0.05$). We classified three types of multi infraorbital foramina as follows: type 1 had one accessory foramen, type 2 had two accessory foramina, and type 3 had three accessory foramina in the infraorbital canal. The infraorbital canal also formed three structures, specifically, a tube-like shape, a funnel shape, and a pinched shape. The accessory canals also contained nerves and blood vessels, and the canals ran downward and supplied the maxillary sinus, teeth, and midfacial region of the craniofacial skeleton, while passing through a few branch canals. These accessory canals proved valuable for blood vessels and nerves and allowed us to recognize the maxilla in the Japanese macaque skull.

Keywords Three-dimensional structure · Skull · Macaque · Maxilla · Infraorbital canal · Posterior superior alveolar canal

T. Zaizen · I. Sato (✉)
Department of Anatomy, School of Life Dentistry at Tokyo, The Nippon Dental University, 1-9-20 Fujimi, Chiyoda-ku, Tokyo 102-8159, Japan
e-mail: iwaoa1@tokyo.ndu.ac.jp

Introduction

Identifying the morphological findings of the infraorbital nerve, such as the terminal branch of the maxillary nerve, is crucial because the nerve must be preserved during maxillofacial surgery (Rath 2001; Hu et al. 2006, 2007). Additionally, knowledge about the distribution of the infraorbital nerve is important for infraorbital nerve blocking with restricted anesthesia (Hwang et al. 2004). Furthermore, the infraorbital canal is an essential morphological feature that is used during facial injections (Lee et al. 2006; Rahman et al. 2009). Traditionally, maxillary nerve blocking has been performed using external anatomic landmarks. However, this morphological approach to nerve identification may be confounded by anatomic variability. Recently, nerve blocking using the CT method (Okuda et al. 2000) and ultrasound imaging (Sola et al. 2012) has been reported, and the need for 3D analysis of the upper jaw has arisen. The existence of multi infraorbital canal foramina has been reported previously, despite its low incidence (5–15 %) (Aziz et al. 2000; Kazkayasi et al. 2001, 2003; Bressan et al. 2004). However, there is no information about assessing the multi infraorbital canal foramina by 3D analysis in humans due to its low incidence. Furthermore, how the presence of the accessory canals affects anesthesia in humans is largely unknown. The accessory canals can be observed in most Japanese macaques. Assessing the presence of the accessory canals in Japanese macaques may lead to findings that are applicable to human dental anesthesia. Therefore, macaques were selected as our model for studying maxilla with multi infraorbital canal foramina using cone-beam computed tomography (CBCT) analysis.

Several elements of the skull of primates, except for the infraorbital canal, have been evaluated via CT scans

(paranasal sinuses, Koppe et al. 1999; Rae and Koppe 2003; development, Zumpano 2002; Zumpano and Richtsmeier 2003). However, there is little information about multi infraorbital foramen for infraorbital nerve and blood vessels. The existence of one or two accessory foramina of the infraorbital canal has been observed in the human skull (Aziz et al. 2000; Kazkayasi et al. 2001, 2003; Bressan et al. 2004). Moreover, the morphological features of the infraorbital canal and accessory bony canals affect the course of the infraorbital nerve and artery supply (Song et al. 2012). However, whether the accessory canals contained blood vessels or nerves has not been reported in detail.

In humans, the infraorbital artery and the posterior superior alveolar artery supply the maxillary sinus, and form an anastomosis in the lateral region wall near the maxillary sinus (Traxler et al. 1999; Solar et al. 1999). The morphology of the infraorbital canal can explain the course and supply of the accessory canals, but it is poorly characterized near the maxillary sinus. Macaques were selected as our model for studying maxilla because they have multi infraorbital canals. Previous reports have shown that knowledge about the arterial supply to the wall of the maxillary sinus is important for surgical methods such as maxillary sinus augmentation and the implantation of bone grafts. Moreover, in humans, there is anastomosis between the posterior superior alveolar artery and the infraorbital artery, which forms a bony canal (Mardinger et al. 2007; Rosano et al. 2011; Song et al. 2012) and complex communications (Traxler et al. 1999; Solar et al. 1999). These bony branch canals contain nerves and blood vessels and may form complex communications in the maxilla during development. The accessory canals of the macaque should be examined because they may be representative of the bony canals of humans. This justifies using the macaque model to test the relationship between the morphology of the multi infraorbital canals and the maxilla structure, which contains the maxillary sinus.

Therefore, in this study, we examined the morphology of the Japanese macaque infraorbital canal, which contains blood vessels and nerves of the maxilla, to determine the detailed course of the infraorbital canal using CBCT.

Materials and methods

This study was performed with 19 adult skulls of Japanese macaques (*Macaca fuscata*), 10 male and 9 female, which were an average age of 6.2 (5–8) years at death. The ages were estimated from their tooth eruption sequence (Iwamoto et al. 1987). These young adult Japanese macaques were supplied for this study by the Department of Anatomy, Nippon Dental University at Tokyo, Japan. The specimens had been fixed in 10 % formalin solution. The heads used for the macroscopic observations of the nerve and blood vessel supply in the infraorbital canal and accessory canals were removed from body. After the specimens were radiographed, they were analyzed.

CBCT imaging

CBCT (PSR 9000N; Asahi Roentgen Industry, Kyoto, Japan) was used in this study. Images of the infraorbital canal and surrounding structures were acquired. The CBCT was operated at a tube potential of 80 kV and a tube current of 4 mA, and the scans were acquired in cylindrical areas of 41 × 40 mm with high resolution (voxel size = 0.1 mm).

Measurements by CBCT images

From the 3D-CBCT images, the diameter of the infraorbital canal was measured using the ASAHI vision software (Asahi Roentgen Industry) and the Micro AVS version 11 software (KGT Industry, Tokyo, Japan). After identifying the median sagittal plane and the palatal plane, the images were defined by using the anterior and posterior nasal spines perpendicular to the median sagittal plane as a reference plane. We tried to analyze whether the infraorbital canal and orbit were important markers of craniofacial parameters in Japanese macaques. The following measurements were then performed. The diameter of the skull was measured by ASAHI vision (Asahi Roentgen Industry) and MicroAVS Version 11 (KGT Industry). The 3D images were produced by INTAGE Realia Professional (KGT Industry). The points measured in the CBCT images of the Japanese macaques are shown in Fig. 1. Six measurements were made for each skull as follows: height from the palatine plane to the superior margin of the orbit (HPP-SMO); width from the midline of the skull to the lateral margin of the orbit (WMS-LMO); height from the palatine plane to the infraorbital foramen (HPP-IOF) and to the accessory foramina (HPP-AF); and width from the midline of the skull to the infraorbital foramen (WMS-IOF) and to the accessory foramina (WMS-AF) (Fig. 1a–f). AF1 is nearest position from the midline of the skull; AF2 is second nearest position from the midline of the skull; AF3 is the farthest position from the midline of the skull. Additionally, we set markers to indicate the ratio occupied by the height of the foramen from the palatine plane, taking 100 to be the height of from the palatine plane to the superior margin of the orbit. We also set markers to indicate the ratio occupied by the width from foramen from the midline of the skull, taking 100 to be the width of the midline of the skull to the lateral margin of the orbit. Index 1 (HPP-IOF/HPP-SMO × 100), Index 2 (HPP-AF1/HPP-SMO × 100), Index 3 (HPP-AF2/HPP-SMO × 100), Index 4 (HPP-AF3/

HPP-SMO × 100), Index 5 (WMS-IOF/WMS-LMO × 100), Index 6 (WMS-AF1/WMS-LMO × 100), Index 7 (WMS-AF2/WMS-LMO × 100), and Index 8 (WMS-AF3/WMS-LMO × 100) were measured.

Statistical methods

The data are reported as the mean ± SD. Statistical analysis was performed using commercially available software (Microsoft® office Excel 2005). Differences between both sides of the skull and sex were analyzed for significance using Student's *t* test after the measurement data were checked for normality. The level of significance was taken to be $P < 0.05$. We used linear regression to correlate the orbit, infraorbital canal and infraorbital foramen. Pearson's correlation coefficient was used to determine the correlations between measurements.

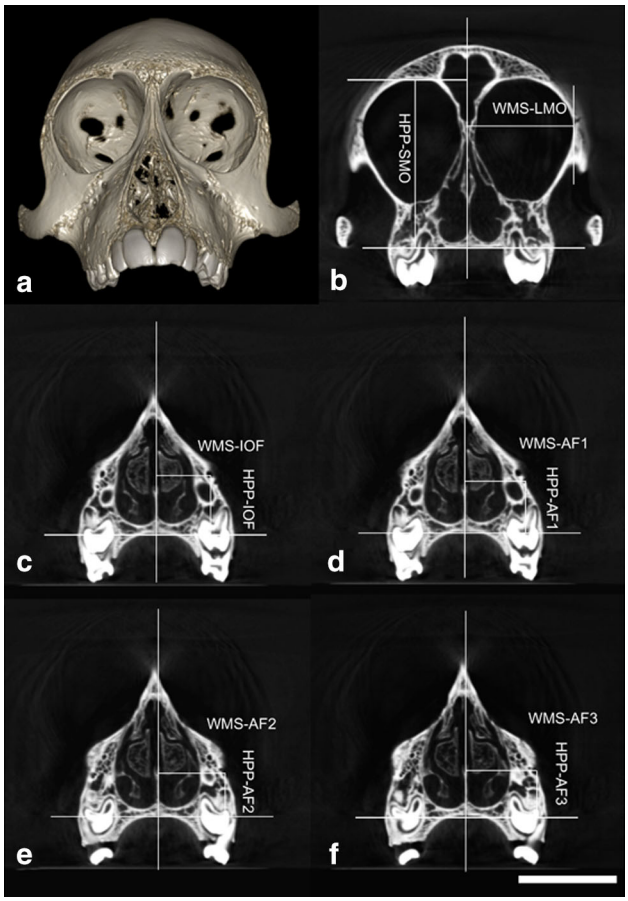

Fig. 1 Measurement points in the frontal view of a cone-beam computed tomography (CBCT) image of a Japanese macaque. **a** Frontal view of 3D image of a Japanese macaque skull. **b** Height from the palatine plane to the superior margin of the orbit (HPP-SMO), and width from the *midline* of the skull to the lateral margin of the orbit (WMS-LMO). **c**, **d**, Height from the palatine plane to the infraorbital foramen (HPP-IOF) and the accessory foramen (HPP-AF1-3), and width from the midline of the skull to the infraorbital foramen (WMS-IOF) and accessory foramen (AF) (WMS-AF1-3). **c** Infraorbital canal (IOC), **d** AF1, **e** AF2, **f** AF3. After identifying the median sagittal plane and the palatal plane, the images were defined using the anterior and posterior nasal spines perpendicular to the median sagittal plane as a reference plane. *Bar* 20 mm

Results

Macroscopic observation of the Japanese macaque maxilla

The infraorbital canal and accessory canals contained some nerves and blood vessels. These canals divided into some branched, bony canals at the maxillary sinus at the posterior region of the maxilla. The nerves and blood vessels that passed through the accessory canals supplied mainly the canines and incisors. The accessory canals were present mainly in a position distant from the midline, compared to the infraorbital foramen (Figs. 2, 3). The infraorbital artery and infraorbital nerve formed anastomosed to the posterior superior alveolar artery, and the posterior superior alveolar nerve passed through bony canals in the posterior region of the Japanese macaque maxilla.

CBCT images of the infraorbital canal and accessory canal

Based on the 3D images of the morphological structure of the infraorbital canal (IOC), we defined three types of infraorbital foramen (IOF) as follows: type 1: one accessory foramen (AF1) (10.5 %, 4/38); type 2: two accessory foramina (AF2) (63.2 %, 24/38); type 3: three accessory foramina (AF3) (26.3 %, 10/38). AC1-2 of types 1 and 2 had a clearly formed canal structure between the surface of the maxilla and the orbit (see Fig. 4) (Figs. 5–7). However, the course of the accessory canals (AC) in type 3 was complex, and no clear canal structure could be discerned (Fig. 7). In Japanese macaques, the IOC and AC run through the maxilla near the maxillary sinus. Specifically, these ACs descend to the cortical bone near the lateral and inferior region near the maxillary sinus. In our images, the IOC and the ACs also gave rise to some small bony canals (Figs. 5, 6, 7, 8) and formed complex communications between the IOC and the ACs in the lateral and inferior regions of the maxilla.

The morphological structure of the IOC can be classified into three shapes as follows: a tube-like shape [39.5 % (15/38); male, 7; female, 8], funnel shape [23.7 % (9/38) male, 6; female, 3], and pinched shape [36.8 % (14/38); male, 7; female, 7]. The structure of the ACs was a funnel shape in most of the specimens examined (Fig. 9).

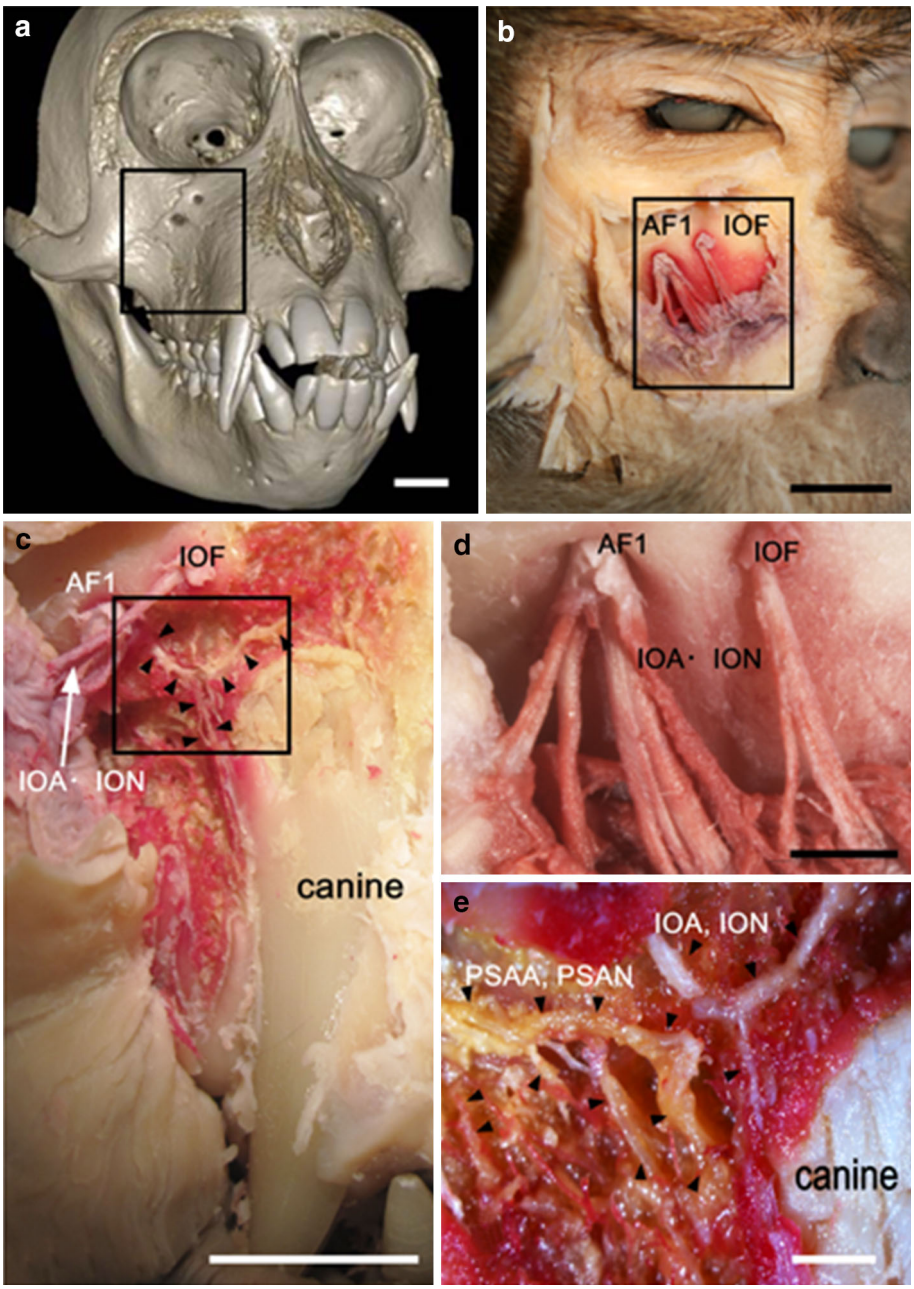

Fig. 2 Frontal view of the head of a Japanese macaque (type 1 see Figs. 3, 4). **a** A type 1 skull CBCT 3D image. The IOF and AF are shown in the right side of the Japanese macaque maxilla. The *squares* in **a** and **b** indicate the same area. **b** IOF and AF after soft tissue dissection of the maxillary region of the Japanese macaque skull. **c** Infraorbital artery and infraorbital nerve supplying the canine and premolar teeth. **d** Larger magnification image of **b**. Some infraorbital arteries and infraorbital nerves supply the soft tissue of the Japanese macaque maxilla though the IOF and AF. **e** Larger magnification of the *square* in **c**. *PSAA* Posterior superior alveolar artery, *PSAN* posterior superior alveolar nerve, *IOC* infraorbital canal, *AF* accessory foramen. *Bars* **a**–**c** 10 mm; **d**, **e** 2 mm

Measurement of the IOF and AF of Japanese macaque maxilla

The measurements of the orbit, IOF and AF (AF1-3) of Japanese macaques are shown in Table 1.

From the measurement results, the AF1 should be located on top of the IOF, but it is located on the side of the nasal cavity. AF2 and AF3 were located further in the nasal cavity than AF1 and were further from the IOF.

A significant correlation was detected between HPP-IOF and HPP-SMO ($r = 0.54$), HPP-AF1 and HPP-SMO ($r = 0.55$), and HPP-AF2 and HPP-SMO ($r = 0.55$) in Japanese macaques. A significant correlation was also detected between WMS-IOF and WMS-LMO ($r = 0.76$), WMS-AF1 and WMS-LMO ($r = 0.57$), WMS-AF2 and WMS-LMO ($r = 0.66$), and WMS-AF3 and WMS-LMO ($r = 0.87$). We found significant sex differences in Index 1 (HPP-IOF/HPP-SMO $\times$ 100) ($P < 0.05$) and Index 2 (HPP-AF1/HPP-SMO $\times$ 100) ($P < 0.05$), but no

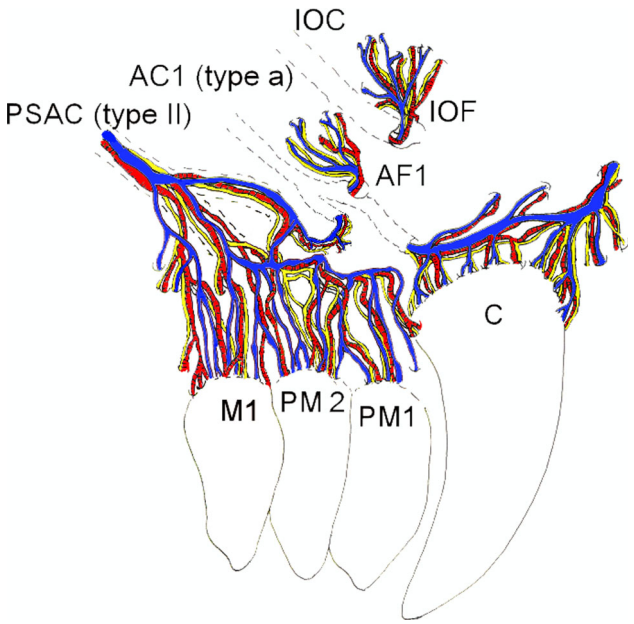

Fig. 3 Illustration of the distribution of the infraorbital artery, infraorbital nerve, posterior superior alveolar artery, and posterior superior alveolar nerve of Fig. 2. The nerves and arteries that develop through the posterior superior alveolar canal connect with other nerves and arteries that pass through the accessory foramen beneath the accessory canal of the infraorbital canal. *AC* Accessory canal, *AF* accessory foramen, *C* canine, *IOC* infraorbital canal, *IOF* infraorbital foramen, *PSAC* posterior superior alveolar canal, *PM1* first premolar, *PM2* second premolar, *M1* first molar

significant differences were found between the measurements on either side of the skull.

Discussion

The existence of multi infraorbital foramina in human skulls has been reported (Aziz et al. 2000; Kazkayasi et al. 2001, 2003; Bressan et al. 2004). However, there is no statistical significance between the locations and length of the infraorbital canal foramen and the size of the human skull, as the course and length of the infraorbital canal foramen can vary greatly (Kazkayasi et al. 2001). We detected a significant correlation between the location and length of the orbit and the IOF or AF in the Japanese macaque. The IOC and ACs affect the course of the infraorbital nerve and artery supply in humans (Song et al. 2012). Scarfe et al. (1998) also suggested that the course of the IOC affects the distribution of the inferior orbital nerve in humans. Therefore, it is expected that the location and distribution of the AFs (or ACs) may affect the supply of blood vessels and nerves in the maxilla of the Japanese macaque. While our measurements showed that the accessory foramina are located on top of the IOF, it is actually located closer to the nasal cavity side. We

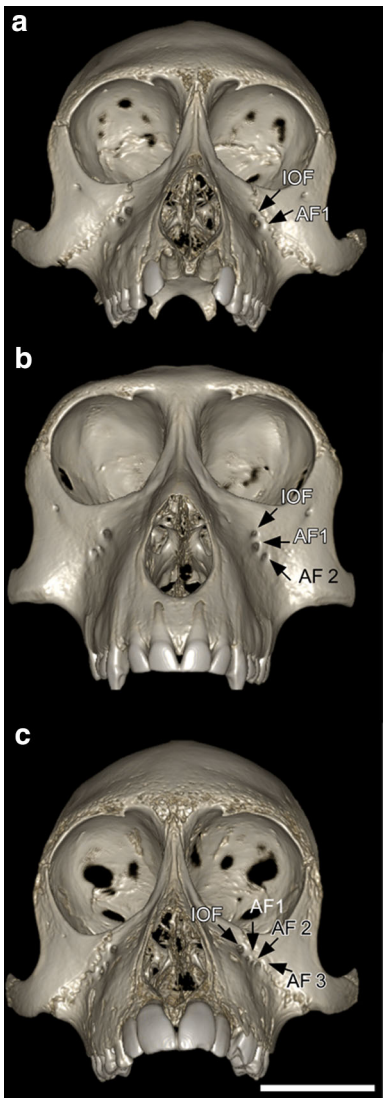

Fig. 4 Three-dimensional CBCT images of the frontal view of a Japanese macaque skull showing the morphological structure of the infraorbital foramen. **a** Type 1: IOF and one AF (AF1). **b** Type 2: IOF and two AF (AF2). **c** Type 3: IOF and three AF (AF3). *Bar* 20 mm

hypothesized that, in humans, the presence of the AF near the nasal cavity indicates the presence of complex bony canals in this area. In the anterior bony region of the maxillary sinus near the nasal cavity, these accessory foramina formed small canals that contained blood vessels and nerves, which supplied the canines and incisors and formed complex communications with each other. Additionally, we found that the bony canal from branches of the IOC is located in the nasal side, further from the IOF. Therefore, these accessory foramina are significant landmarks for the complex communication of the nerves or blood vessels.

Matsukawa et al. (1969) reported the complex course of the infraorbital artery and posterior superior alveolar artery using injection acrylic resin and found that a few arterial

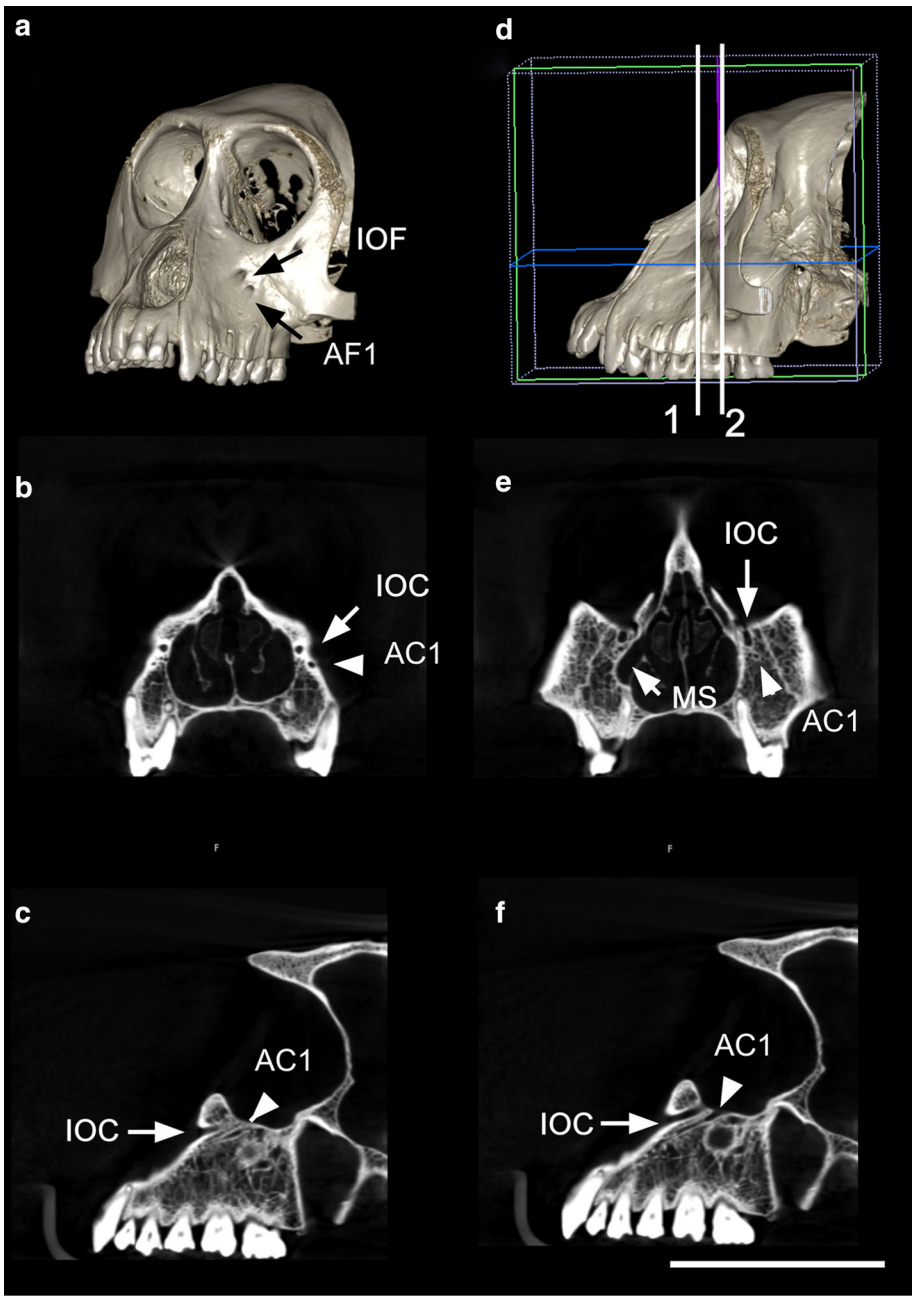

Fig. 5 The morphological structure of a type 1 IOF and AC (or AF), as determined by 3D CBCT images and sections of CBCT images. **a** 3D morphological structure of the left side of the skull. IOF (*arrow*) and one AF1 (*arrow*) are shown in the front-lateral view of the Japanese macaque maxilla. **b** Frontal section CBCT image of a Japanese macaque skull. A bony IOC (*arrow*) and AC1 (*arrowhead*) were found from the entrance of the maxilla to the subfissure orbit small hole. The IOC and one AC1 (*arrowhead*) are shown in the maxilla. The IOC(*arrow*) and one AC (*arrowhead*) are shown in the Japanese macaque frontal section of the maxilla, 3 mm interior to the IOC entrance (*line 2* frontal section of skull). **c** Sagittal section of a Japanese macaque skull. The entrances to the bony canals of the IOC (*arrow*) and the bony AC (AC1, *arrowhead*) are shown as small tunnels in the same position as in **b**. **d** Lateral 3D view of the left side of a Japanese macaque skull. The *vertical and frontal lines* indicate the observed positions of the IOC and AC, respectively. Two *frontal lines* are also shown in the 3D image of the skull. **e** Frontal section CBCT image of a Japanese macaque skull. The IOC (*arrow*) and AC (AC1, *arrowhead*) were found at the lateral surface of the maxillary sinus (MS, *arrow*) in the positions indicated in **d**. The *small hole* or semicircular structure of the subfissure orbit is shown. **f** Sagittal section of a Japanese macaque skull in the position indicated in **d**. The entrances of the bony canals of the IOC (*arrow*) and bony AC (*arrowhead*) are shown as small tunnels. *Bar* 20 mm (**a** and **d** are the same magnification; **b**, **c**, **e**, and **f** are the same magnification)

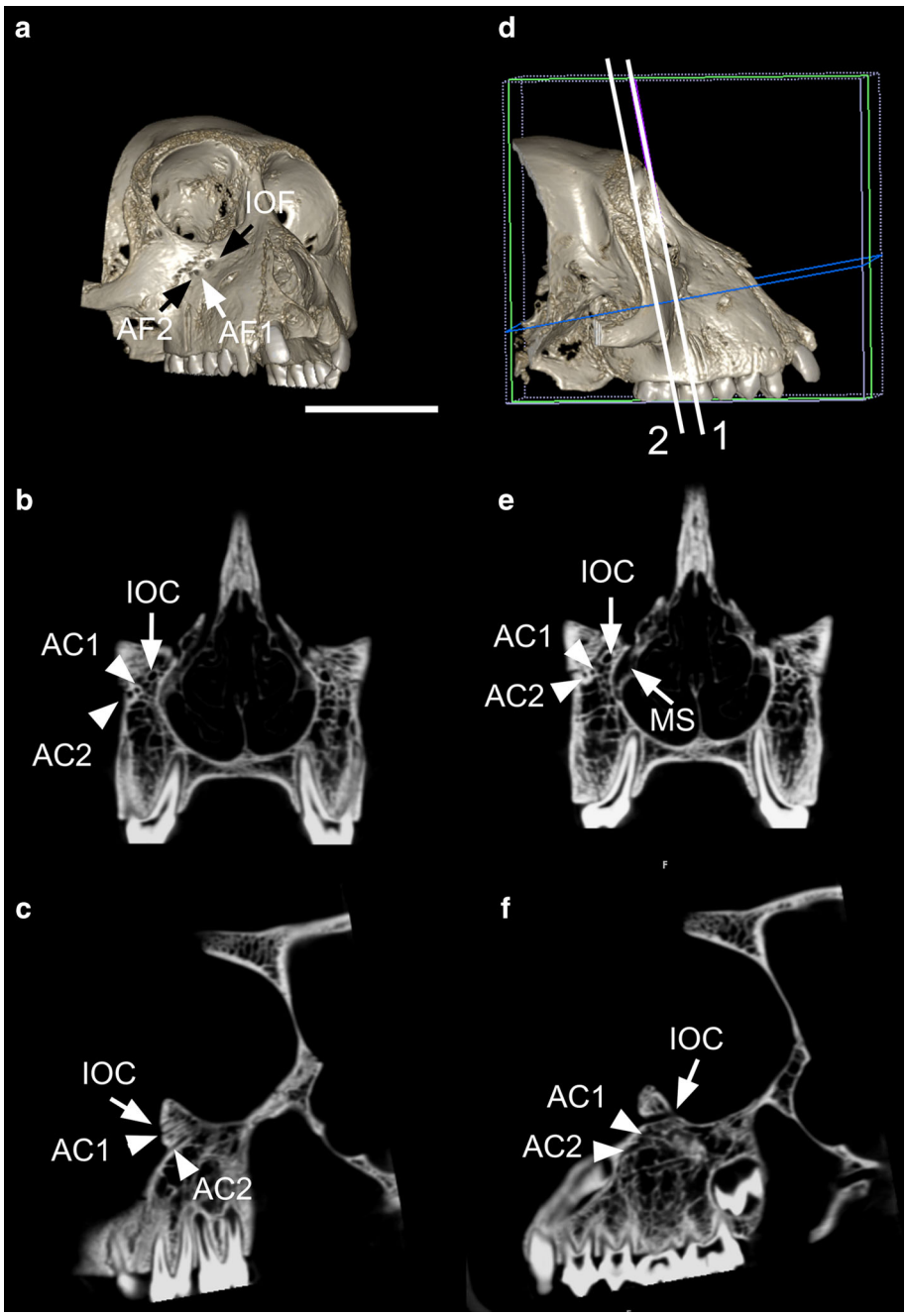

Fig. 6 The morphological structure of a type 2 IOC and AC, as shown by 3D CBCT images and sections of CBCT images. **a** 3D morphological structure of the right side of the skull. The IOF (*arrow*) and two AFs (AF1-2, *arrowheads*) are shown in the front-lateral view of the maxilla. **b** Frontal section CBCT image of a Japanese macaque skull. The bony IOC (*arrow*) and AC1-2 (*arrowheads*) originated from the entrance of the maxilla. The IOC and ACs (AC1-2, *arrowheads*) are shown in the maxilla. The IOC (*arrow*) and two ACs (AC1-2, *arrowheads*) are shown in the frontal section of the maxilla, 2 mm inside the IOC entrance. **c** Sagittal section of a Japanese macaque skull. The entrances of the bony canals of the IOC (*arrow*) and bony ACs (AC1-2, *arrowheads*) are shown as thin tunnels in the same positions as in **b**. **d** Lateral 3D view of the right side of a Japanese macaque skull. The *vertical and horizontal lines* indicate the observed positions of the IOC and AC, respectively. **e** Frontal section CBCT image of a Japanese macaque skull. The IOC (*arrow*) and two ACs (AC1-2, *arrowhead*) were found at the lateral or lateral-superior of the maxillary sinus (MS, *arrow*) in the positions indicated in Fig. 3d. The *small hole* structure of these tunnels is shown. **f** Sagittal section of a Japanese macaque skull in the position indicated in **d**. The entrances of the bony canals of the IOC (*arrow*) and bony ACs (AC1-2, *arrowheads*) are shown as small tunnels. *Bar* 20 mm (**a** and **d** are the same magnification; **b**, **c**, **e**, and **f** are the same magnification)

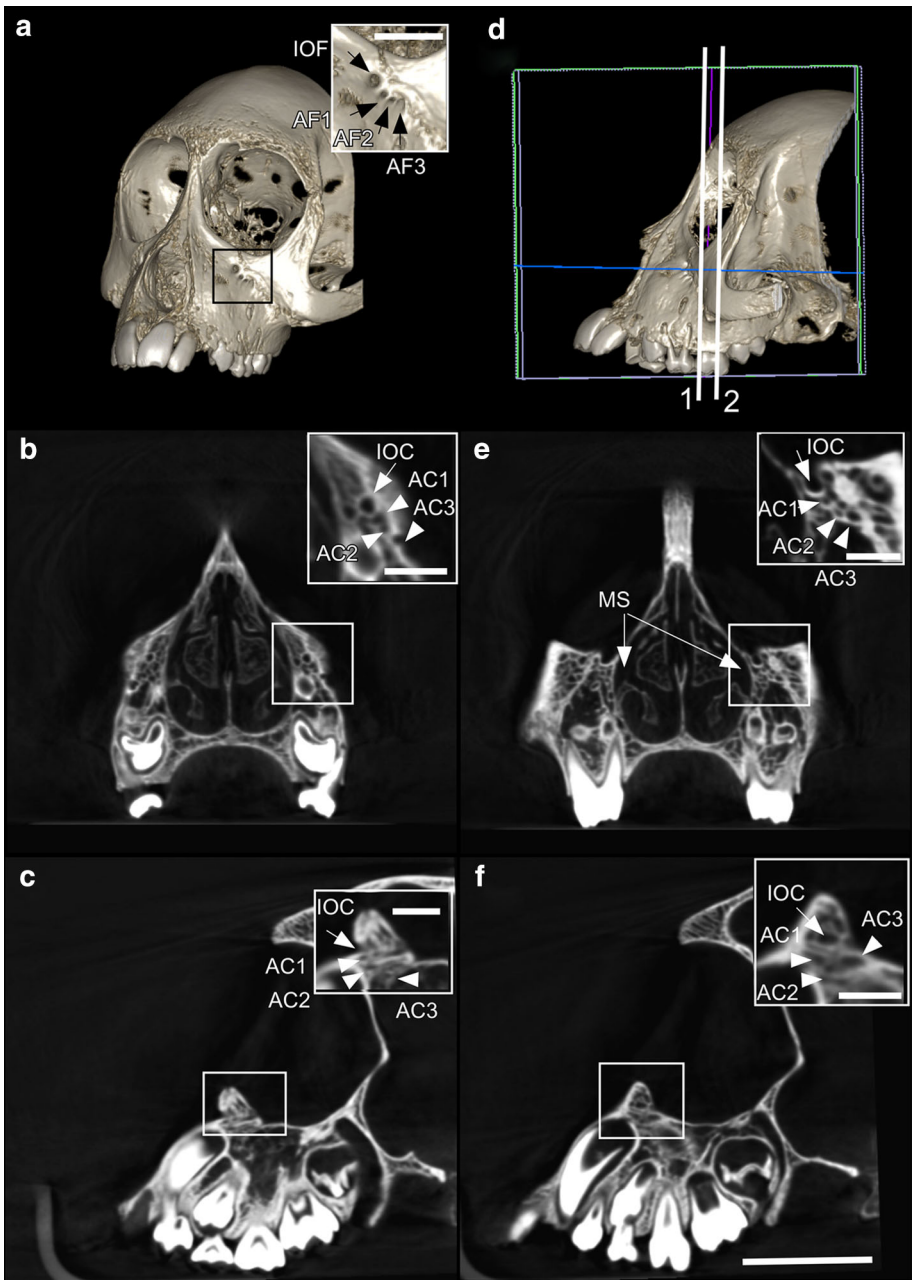

Fig. 7 The morphological structure of a type 3 IOC and AC, as shown by 3D CBCT images and sections of CBCT images. **a** 3D morphological structure of the left side of the skull. The IOF (*arrow*) and three AF (AF1-3, *arrowheads*) are shown in the large magnification of the *square* (*Bar* 5 mm). **b** Frontal section CBCT image of a Japanese macaque skull. The bony IOC (*arrow*) and three ACs (AC1-3, *arrowheads*) originated from the entrance of the maxilla. The IOC and three ACs (AC1-3, *arrowheads*) are shown in the maxilla. The IOC (*arrow*) and three ACs (AC1-3, *arrowheads*) are shown in the frontal section of the maxilla, 3 mm inside the IOC entrance in the magnification of the *square* (*Bar* 5 mm) in Fig. 4b. **c** Sagittal section of a Japanese macaque skull. The entrance of the bony canals of the IOC (*arrow*) and bony AC (AC1-3, *arrowheads*) are shown as thin tunnels in the same position as in Fig. 4b. These tunnels run a complex route in the magnification of the *square* (*Bar* 5 mm) in **c**. **d** Lateral 3D view of the right side of the skull. The *vertical and horizontal lines* indicate the observed positions of the IOC and AC, respectively. **e** Frontal section CBCT image of a Japanese macaque skull. The IOC (*arrow*) and AC (AC1-3, *arrowhead*) were found at the lateral-superior of the maxillary sinus (MS, *arrow*) in the positions indicated in Fig. 4d. The small hole structure of these tunnels is shown in the magnification of the *square* (*Bar* 5 mm) in **e**. **f** Sagittal section of a Japanese macaque skull in the position indicated in **d**. The entrance of the bony canals of the IOC (*arrow*) and bony ACs (AC1-3, *arrowheads*) are shown as small tunnels in the magnification of the *square* (*Bar* 5 mm) in **f**. *Bar* 20 mm (**a** and **d** are the same magnification; **b**, **c**, **e**, and **f** are the same magnification)

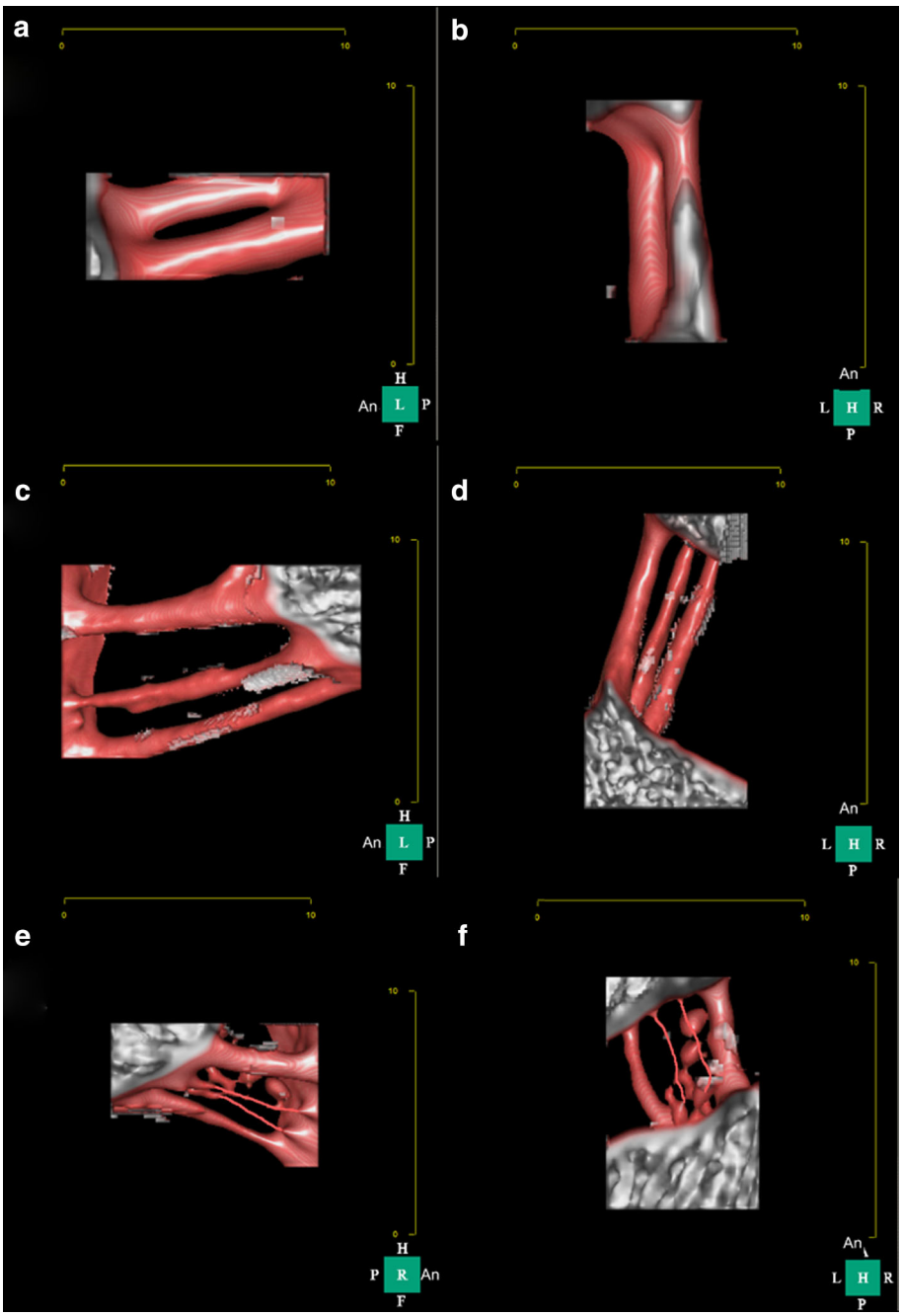

Fig. 8 Three types of IOC and AC structures from 3D CBCT images of Japanese macaque. **a** Sagittal view of the double-canal shape of the IOC and AC of type 1. The tube-like shape of the canal is relatively uniform in the IOC and AC. **b** Horizontal view of the double-canal shape of the IOC and AC of type 1. **c** Sagittal view of the triple-canal shape of the IOC and AC of type 2. The tunnel diameter decreases gradually as it approaches the IOF. **d** Horizontal view of the triple-canal shape of the IOF and AC of type 2. **e** Sagittal view of the four-canal shape of the IOC and AC of type 3. The multiple canal shape forms a complex tunnel. **f** Horizontal view of the four-canal shape of the IOC and AC of type 3. *A*, anterior surface; *H*, superior surface; *F*, inferior surface; *L*, left side; *R*, right side; *P*, posterior surface; *Bar* 10 mm

resources run to the bony wall in the Japanese macaque maxilla. However, the distribution of blood vessels and the course of the blood vessels leading to the bone were not clear in their report, as large parts of bone material was lost. In our study, the courses of the IOC, posterior superior alveolar canal and accessory canal in the Japanese macaques were observed using CBCT; the existence of blood vessels and nerves in the AF was also assessed by macroscopic observation. The human skull has one or more accessory foramina 10 % (one 5 %; two 5 %) (Kazkayasi et al. 2001, 2003), 4.7 % (Bressan et al. 2004), 15 % (Aziz et al. 2000). We found multiple accessory foramina in all of the Japanese macaques examined. The blood vessels and nerves originating from these accessory foramina depended on the course of the bony canal, and the blood vessel and nerve supplies might be limited compared to human anastomosed nerves or blood vessels. Therefore, these multiple accessory foramen affect the course of the bony canal, which contains blood vessels and nerves in the maxilla.

A number of factors, such as the size of the teeth and the size of the brain and skull, might account for this difference between humans and Japanese macaques. The presence of multiple IOCs in the Japanese macaque may also

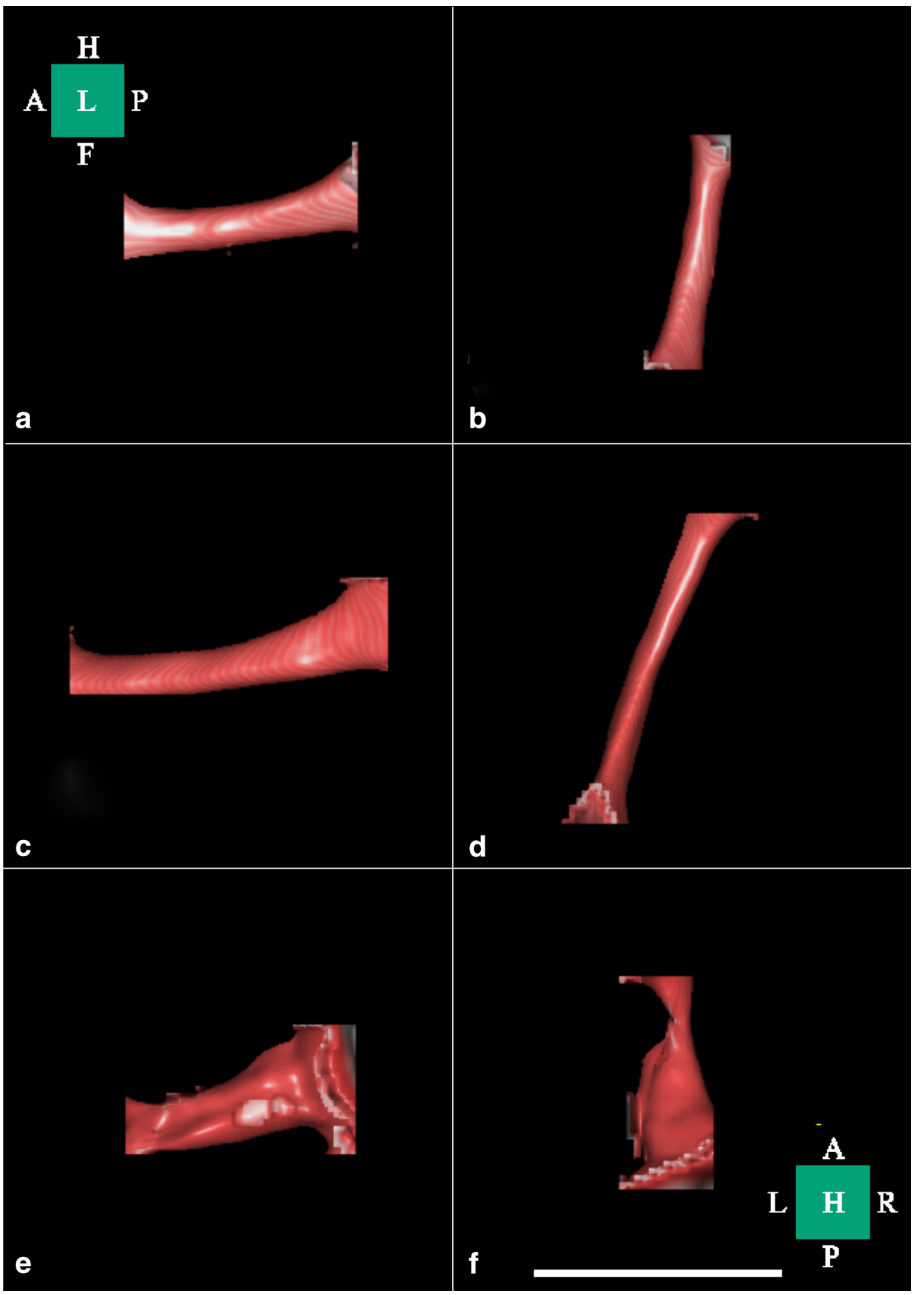

Fig. 9 The IOC structure of 3D CBCT images of a Japanese macaque. **a** Sagittal view of the tube-like shape of the IOC. **b** Horizontal view of the tube-like shape of the IOC. **c** Sagittal view of the funnel shape of the IOC. The tunnel diameter decreases gradually as it approaches the IOF. **d** Horizontal view of the funnel shape of the IOC. **e** Sagittal view of the pinched shape of the IOC. The tunnel is narrow and pinched as it approaches the IOF. **f** Horizontal view of the pinched shape of the IOC. *Bar* 10 mm

contribute to these differences. The infraorbital groove, IOC, and IOF are also important landmarks for the morphological analysis of skulls (Kazkayasi et al. 2001). The

IOC and the orbit are also important markers of craniofacial parameters in mammals (Olopade and Onwuka 2009). Therefore, we tried to analyze the correlation between the IOF or AF1-3 and the orbit of the skull in Japanese macaques. However, a significant difference between sexes was found only in Index 1 and Index 2, but no significant differences were observed between the measurements on either side of the skull. Therefore, it is unlikely that these markers and factors determine the craniofacial parameters of the Japanese macaque, but they may instead indicate the distribution of blood vessels and nerves in the maxilla. The morphological structure of the 3D images of the human IOC was classified into the three following types: a tube-like shape (69 %; 58/84), a funnel shape (25 %; 21/84), and a pinched shape (6 %; 5/84) (Lee et al. 2006). In this study, the morphological structure of the Japanese macaque IOC was also classified into the three following types: a tube-like shape [39.5 % (15/38)], funnel shape [23.7 % (9/38)], and pinched shape [36.8 % (14/38)]. The funnel and pinched shape of the infraorbital canal were found mainly in Japanese macaque, but not in

Table 1 Diameter of the IOC measured using three-dimensional cone-beam computed tomography (3D-CBCT)

Total (mean ± SD)		Sex		Sides	
		Male	Female	Right	Left
HPP-SMO	25.6 ± 2.0	26.34 ± 2.0	24.83 ± 1.83	25.7 ± 2.11	25.5 ± 2.03
HPP-IOF	24.1 ± 3.5	25.2 ± 2.7	22.9 ± 3.8	24.4 ± 3.4	23.9 ± 3.6
HPP-AF 1	18.7 ± 3.6	19.7 ± 3.3	17.48 ± 3.8	18.7 ± 3.0	18.6 ± 4.3
HPP-AF 2	16.2 ± 2.5	16.5 ± 2.3	15.8 ± 2.8	15.7 ± 2.9	16.7 ± 2.0
HPP-AF3	16.6 ± 2.5	14.9 ± 0.8	18.3 ± 5.5	14.7 ± 1.0	17.8 ± 4.9
WMS-LMO	43.5 ± 3.0	44.6 ± 2.7	42.4 ± 2.99	43.6 ± 3.0	43.5 ± 3.1
WMS-IOF	53.2 ± 3.3	53.8 ± 2.9	52.5 ± 3.7	52.0 ± 2.8	54.3 ± 3.4
WMS-AF1	57.5 ± 5.4	58.8 ± 4.3	56.1 ± 6.2	55.9 ± 4.9	59.2 ± 5.4
WMS-AF2	62.7 ± 4.7	63.6 ± 4.0	61.6 ± 5.4	61.5 ± 4.1	64.1 ± 5.0
WMS-AF3	62.1 ± 2.8	62.4 ± 3.3	61.9 ± 2.7	62.9 ± 2.7	61.6 ± 3.1

Six measurements (mm) were made for each skull: *HPP-SMO* height from the palatine plane to the superior margin of the orbit, *WMS-LMO* width from the midline of the skull to the lateral margin of the orbit, *HPP-IOF* height from the palatine plane to the infraorbital foramen, *HPP-AF1-3* height from the palatine plane to the accessory foramina, *WMS-IOF* width from the midline of the skull to the infraorbital foramen, *WMS-AF1-3* width from the midline of the skull to the accessory foramina

humans. These results also suggest that the accessory foramina affected the development of the skull in Japanese macaques. The course of the Japanese macaque IOC with AF1 and AF2 is simple and runs straight from the orbit to front surface of the maxilla. In contrast, in the maxilla, the course of the IOC with AF3 is complex. We propose that the courses of ACs of the IOC are controlled by the structure of the maxilla. The IOC and ACs, which contain numerous vessels and nerves, are spread out in the narrow space of the maxilla during the formation of the skull. The course of the bony canal and its branches has been identified at the maxillary sinus in human and was shown to occur in 62.2 % (23 of 37 skulls) (Murakami et al. 1994), 55 % (114 of 208 skulls) (Mardinger et al. 2007), and 47 % (94 of 200 skulls) (Rosano et al. 2011). In our study of Japanese macaques, the IOC and AC were found in the maxilla near the maxillary sinus. In Japanese macaques, the branches of the IOC and accessory foramina might form both blood and nervous supplies in the maxilla. The accessory foramina can also divide into multi bony canals, which contain blood vessels and nerves supplying the lateral-inferior area of the infraorbital canal. Therefore, the existence of accessory foramina is one of the most important landmarks for the supply vessels and nerves in the maxillary sinus in Japanese macaque. The canines are also located in this area, and more blood vessels and nerves supply the large canine area in Japanese macaques compared to humans. The course of the IOC and ACs, such as the branching of the bony canal, also affects the morphology of the maxillary sinus in Japanese macaques.

Conflict of interest None.

References

Aziz SR, Marchena JM, Puran A (2000) Anatomic characteristics of the infraorbital foramen: a cadaver study. J Oral Maxillofac Surg 58:992–996

Bressan C, Geuna S, Malerba G, Giacobini G, Giordano M, Robecchi MG, Vercellino V (2004) Descriptive and topographic anatomy of the accessory infraorbital foramen. Clinical implications in maxillary surgery. Minerva Stomatol 53:495–505

Hu KS, Kwak HH, Song WC, Kang HJ, Kim HC, Fontaine C, Kim HJ (2006) Branching patterns of the infraorbital nerve and topography within the infraorbital space. J Craniofac Surg 17:1111–1115

Hu KS, Kwak J, Koh KS, Abe S, Fontaine C, Kim HJ (2007) Topographic distribution area of the infraorbital nerve. Surg Radiol Anat 29:383–388

Hwang K, Suh MS, Chung IH (2004) Cutaneous distribution of infraorbital nerve. J Craniofac Surg 15:3–5

Iwamoto M, Watanabe T, Hamada Y (1987) Eruption of permanent teeth in Japanese monkeys (*Macaca fuscata*). Primate Res 3:18–28

Kazkayasi M, Ergin A, Ersoy M, Bengi O, Tekdemir I, Elhan A (2001) Certain anatomic relations and precise morphometry of the infraorbital foramen-canal and groove: an anatomical and cephalometric study. Laryngoscope 111:609–614

Kazkayasi M, Ergin A, Ersoy M, Tekdemir I, Elhan A (2003) Microscopic anatomy of the infraorbital canal, nerve, and foramen. Otolaryngol Head Neck Surg 129:692–697

Koppe T, Rae TC, Swindler DR (1999) Influence of craniofacial morphology on primate paranasal pneumatization. Ann Anat 181:77–80

Lee UY, Nam SH, Choi KN, Kim TJ (2006) Morphologic characteristics of the infraorbital foramen and infraorbital canal using three-dimensional models. Surg Radiol Anat 28:115–120

Mardinger O, Abba M, Hirshberg A, Schwartz-Arad D (2007) Prevalence, diameter and course of the maxillary intraosseous vascular canal with relation to sinus augmentation procedure: a radiographic study. Int J Oral Maxillofac Surg 36:735–738

Matsukawa M, Ryumon A, Furuhara H, Masuda S (1969) Stereological studies on several ducts and vessels by injection method

of acrylic resin. XXII. On the superficial temporal artery of Macacus cynomolgos. Okajimas Folia Anat Jpn 45:267–278

Murakami G, Ohtsuka K, Sato I, Moriyama H, Shimada K, Tomita H (1994) The superior alveolar nerves: their topographical relationship and distribution to the maxillary sinus in human adults. Okajimas Folia Anat Jpn 70:319–328

Okuda Y, Okuda K, Shinohara M, Kitajima T (2000) Use of computed tomography for maxillary nerve block in the treatment of trigeminal neuralgia. Reg Anesth Pain Med 25:417–419

Olopade JO, Onwuka SK (2009) Morphometric analysis of the skull of the Sahel goat breed: basic and clinical anatomy. Ital. J Anat Embryol 114:167–178

Rae TC, Koppe T (2003) The term "lateral recess" and craniofacial pneumatization in old world monkeys (Mammalia, Primates, Cercopithecoidea). J Morphol 258:193–199

Rahman M, Richter EO, Osawa S, Rhoton AL (2009) Anatomic study of the infraorbital foramen for radiofrequency neurotomy of the infraorbital nerve. Neurosurgery 64:423–428

Rath EM (2001) Surgical treatment of maxillary nerve injuries. The infraorbital nerve. Atlas Oral Maxillofac Surg Clin North Am 9:31–41

Rosano G, Taschieri S, Gaudy JF, Weinstein T, Del Fabbro M (2011) Maxillary sinus vascular anatomy and its relation to sinus lift surgery. Clin Oral Implants Res 22:711–715

Scarfe WC, Langlais RP, Ohba T, Kawamata A, Maselle I (1998) Panoramic radiographic patterns of the infraorbital canal and anterior superior dental plexus. Dentomaxillofac Radiol 27:85–92

Sola C, Raux O, Savath L, Macq C, Capdevila X, Dadure C (2012) Ultrasound guidance characteristics and efficiency of suprazygomatic maxillary nerve blocks in infants: a descriptive prospective study. Pediatric Anesthesia 22:841–846

Solar P, Geyerhofer U, Traxler H, Windisch A, Ulm C, Watzek G (1999) Blood supply to the maxillary sinus relevant to sinus floor elevation procedures. Clin Oral Implants Res 10:34–44

Song WC, Kim JN, Yoo JY, Lee JY, Won SY, Hu KS, Kim HJ, Koh KS (2012) Microanatomy of the infraorbital canal and its connecting canals in the maxilla using 3-D reconstruction of microcomputed tomographic images. J Craniofac Surg 23:1184–1187

Traxler H, Windisch A, Geyerhofer U, Surd R, Solar P, Firbas W (1999) Arterial blood supply of the maxillary sinus. Clin Anat 12:417–421

Zumpano MP (2002) Size and shape changes during late fetal growth (137–157 gestational days) in the pigtailed macaque (*Macaca nemestrina*) craniofacial complex: an application using three-dimensional coordinate data and finite element scaling analysis. Anat Rec 267:307–320

Zumpano MP, Richtsmeier JT (2003) Growth-related shape changes in the fetal craniofacial complex of humans (*Homo sapiens*) and pigtailed macaques (*Macaca nemestrina*): a 3D-CT comparative analysis. Am J Phys Anthropol 120:339–351